

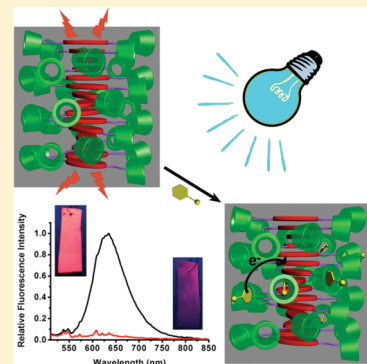
# Reversible and Selective Sensing of Aniline Vapor by Perylene-Bridged Bis(cyclodextrins) Assembly

Bang-Ping Jiang, Dong-Sheng Guo, and Yu Liu\*

Department of Chemistry, State Key Laboratory of Elemento-Organic Chemistry, Nankai University, Tianjin 300071, P. R. China

**S** Supporting Information

**ABSTRACT:** Detecting volatile amines is a significant topic in quality control of food and medical diagnosis. Selectively sensing a given gaseous amine from other analogues, however, still remains a formidable challenge in solid-state fluorescence sensing because of the lack of specialized binding sites. Herein, we demonstrate a new supramolecular strategy for selectively sensing aniline based on the aggregation of perylene-cyclodextrin conjugate **1**. Compared with our previous results based on perylene-bridged bis(permethyl- $\beta$ -cyclodextrins), the present system achieves a pronounced improvement of both selectivity and reversibility. The sensory material was constructed from the  $\pi$ -stacking aggregate of **1** embedded in poly(vinylidene fluoride) membrane, which ensures benign solid-state fluorescence with potential amplification mechanism as well as convenient preparation and practical operation. Grafting cyclodextrin receptors endows the sensory material with desired selectivity as a result of diverse binding abilities. Especially, the thermodynamically reversible host–guest inclusion leads to the excellent sensing reversibility. The present research opens the way to build new n-type fluorescence sensory materials for detecting volatile amines instantly with compelling selectivity, sensitivity, and reversibility.



## INTRODUCTION

Fluorescence sensory materials based on conjugated polymers have gained considerable attention since the seminal work by Swager's group,<sup>1</sup> showing several significant advantages: mainly signal amplification, as well as easy fabrication of devices and potential combination of outputs.<sup>2</sup> More importantly, such amplifying fluorescent polymers are proven to be effective in sensing vapors of volatile organic compounds via super-quenching.<sup>3</sup> Up to now, much more attention has been paid to p-type materials, which are suited for sensing oxidative reagents,<sup>3a,4</sup> whereas the corresponding investigation on n-type materials, suited for sensing reducing reagents, has been reported much less frequently.<sup>5</sup> Zang and co-workers successfully developed a new n-type sensory material based on  $\pi \cdots \pi$  aggregation of electron-poor perylene for vapor probing of organic amines.<sup>6</sup>

Volatile amines are a byproduct of rapidly growing cells and commonly produced by organic decomposition.<sup>7</sup> Some volatile amines are considered as quality indicators of foodstuffs such as meats,<sup>8</sup> cheeses,<sup>9</sup> and other foods. Additionally, others are usually used as biomarkers in certain types of diseases, for example, aniline and o-toluidine have been reported to be biomarkers for patients having lung cancer,<sup>10</sup> whereas dimethylamine and trimethylamine have been reported to be the cause of the "fishy" uremic breath odor experienced by patients with renal failure.<sup>11</sup> Therefore, detecting volatile amines not only is critical to quality control of food but also may provide expedient ways for medical diagnosis. However, to the best of our knowledge, it still remains a severe challenge to be addressed that selectively detecting and distinguishing a given gaseous amine from other analogues, due

to the lack of specialized binding sites in sensory materials.<sup>12</sup> The introduction of well-defined receptor sites in building sensory materials is very rare, although displaying potential advantages for selectively sensing organic vapors.<sup>13</sup>

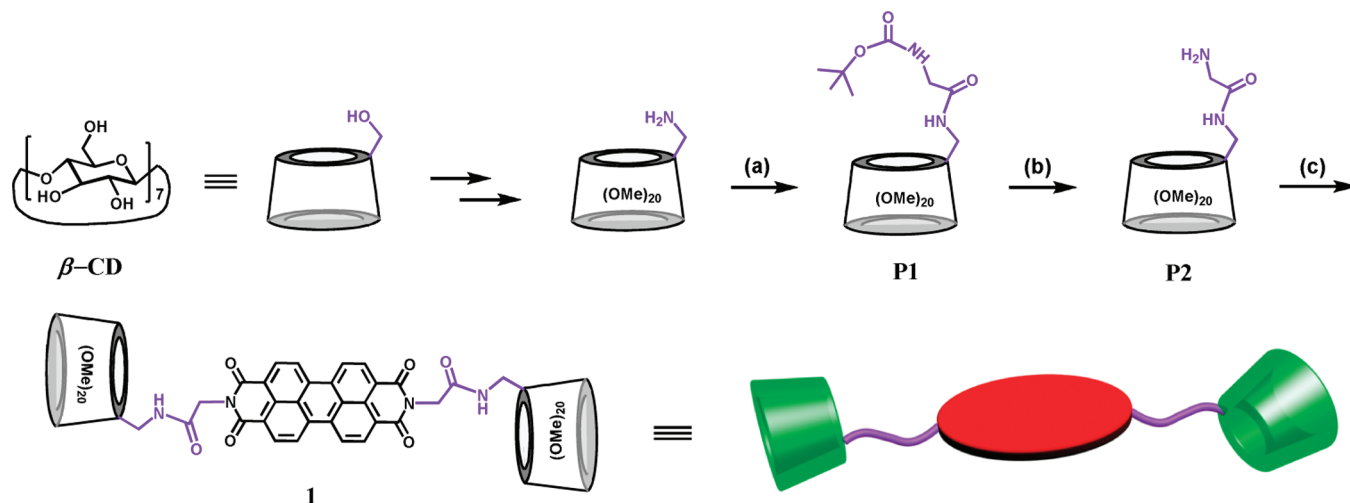
In the present work, we provided the highly reversible solid-state fluorescence sensory material **1** (Scheme 1) by grafting perylene bisimides (PBI) with cyclodextrin (CD). The aggregated fluorescence of PBI serves as probing signal, and CD serves as receptor unit. As a result, the membrane-embedded **1** in poly(vinylidene fluoride) (PVDF) can probe aniline vapor with high selectivity and sensitivity, benefiting from the inclusion diversity of the CD cavity and the amplification mechanism based on desired aggregation performance of PBI backbones.

## RESULTS AND DISCUSSION

**Aggregation Capability of 1.** PBI-bridged bis(permethyl- $\beta$ -CDs) **1** was synthesized from 6-deoxy-6-amino-permethyl- $\beta$ -CD<sup>14</sup> through three reactive steps as shown in Scheme 1. First, the precursor **P1** was synthesized according to condensation reaction between 6-deoxy-6-amino-permethyl- $\beta$ -CD and *N*-(*tert*-butoxycarbonyl)-glycine.<sup>15</sup> Subsequent removal of the *t*-BOC of **P1** was accomplished by CF<sub>3</sub>COOH to give **P2**. Finally, the condensation of **P2** with perylene tetracarboxylic bisanhydride in the presence of Zn(CH<sub>3</sub>COO)<sub>2</sub> as catalyst afforded the target compound **1** in 34% yield. PBI and its derivatives represent a

**Received:** April 12, 2011

**Published:** June 27, 2011

Scheme 1. Synthetic Route and Structural Illustration of **1**<sup>a</sup>

<sup>a</sup> Conditions and reagents: (a) *N*-(*tert*-butoxycarbonyl)-glycine, DCC, HOBT, and THF; (b) trifluoroacetic acid and dichloromethane; (c) perylene-3,4,9,10-tetracarboxylic acid bisanhydride, zinc acetate, and imidazole, 140 °C.

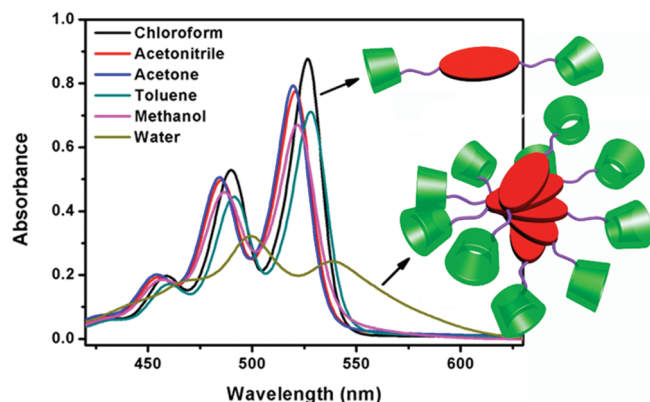


**Figure 1.** UV-vis spectra of **1** ( $1.0 \times 10^{-5}$  M) in different solvents at 25 °C. Inset: monomeric form in chloroform and aggregated form in water.

robust class of n-type organic materials with strong fluorescence, which is particularly desirable for use in optical sensing or probing in regard to both the thermal and photochemical stabilities.<sup>16</sup> CDs, a class of cyclic oligosaccharides with six to eight D-glucose units linked by  $\alpha$ -1,4-glucose bonds, possess size-exclusion cavities with the capability of capturing various substrate molecules.<sup>17</sup>

It is well-known that the  $\pi \cdots \pi$  aggregation of PBI is solvent-dependent.<sup>16a</sup> Stronger  $\pi$ -stacking promotes a longer-range molecular arrangement, which is highly favorable for exciton migration via cofacial intermolecular electronic coupling.<sup>6a</sup> Facile exciton migration can be effectively disturbed by less occupation of integrated receptor units, enabling amplification in fluorescence quenching.<sup>17,2a</sup> Therefore, we primarily studied the aggregation behaviors of **1** in different solvents. UV-vis spectra of **1** (Figure 1) show three distinguishable absorption bands between 450 and 550 nm with the maximal absorptivity at the first band in organic solvents (chloroform, acetonitrile, acetone, toluene, and methanol), indicating the typical nonaggregated or low aggregated state of **1**. The spectrum of **1** decreases evidently and becomes broader in water, with the maximal absorptivity at the

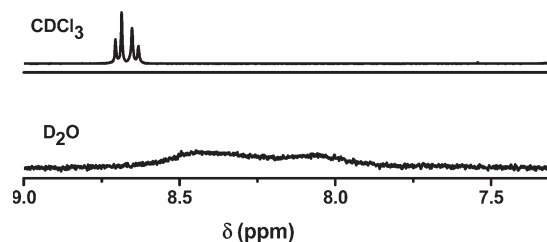


**Figure 2.** <sup>1</sup>H NMR spectra of **1** in CDCl<sub>3</sub> and D<sub>2</sub>O, respectively.

second band, indicating the pronounced  $\pi$ -stacking aggregation of PBI backbones. The quantitative aggregation constant of **1** in water was obtained as  $2.1 \times 10^6 \text{ M}^{-1}$  (Figure S11 in Supporting Information) using a nonlinear least-squares regression analysis of the concentration-dependent UV-vis spectral data by the isodesmic or equal-K model,<sup>18</sup> illustrating aggregation ability 1–2 orders of magnitude stronger than that of previous CD-PBI derivatives.<sup>13a,19</sup> The elongated spacer in **1** avoids effectively the unfavorable steric hindrance of CD units for  $\pi$ -stacking.

The strong  $\pi$ -stacking of **1** in water was also validated by NMR experiments. <sup>1</sup>H NMR spectra of **1** were comparatively performed in CDCl<sub>3</sub> and D<sub>2</sub>O (Figure 2). In CDCl<sub>3</sub>, a simple pattern of sharp signals for the PBI protons is observed, showing that **1** exists in the monomeric form at such a high concentration of 3 mM, whereas in D<sub>2</sub>O, the signals are drastically broadened and suffer pronounced upfield shifts as a result of the  $\pi$ -stacking ring current.<sup>20</sup> Therefore, based on the results of UV-vis and NMR experiments, we used water as solvent medium in the following experiments to favor strong  $\pi \cdots \pi$  aggregation. X-ray powder diffraction (XRD) measurement of **1** from aqueous solution showed one strong peak at  $2\theta = 11.08^\circ$ , with three smaller peaks at  $26.64^\circ$ ,  $27.94^\circ$ , and  $30.94^\circ$ , and the *d* values were determined to be 8.00, 3.34, 3.19, and 2.89 Å from these peaks (Figure S12 in Supporting Information). Referring to the  $\pi$ -stacking distances between neighboring PBI moieties (3.34–3.55 Å),<sup>21</sup> a *d* value of 3.34 Å was assigned to the  $\pi$ -stacking distance of **1**, which is somewhat smaller than the common  $\pi$ -stacking distances (3.50 Å) of PBI derivatives,<sup>16a</sup> possibly

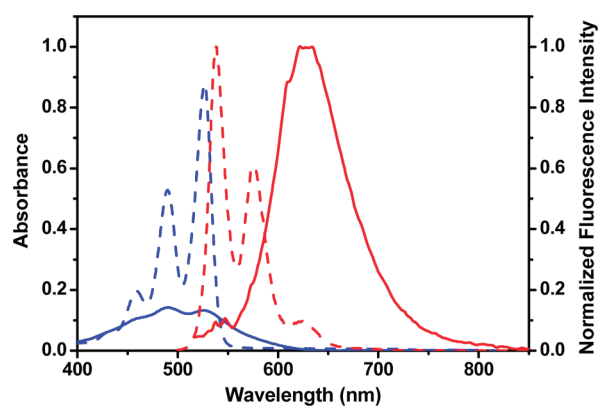


Figure 3. UV-vis (blue) and fluorescence (red) spectra of **1** in chloroform ( $1.0 \times 10^{-5}$  M) (dashed) and the PVDF-embedded **1** (solid),  $\lambda_{\text{ex}} = 490$  nm.

owing to the cooperative contribution of intermolecular hydrogen bonding between amide spacers (proved by FT-IR spectroscopy, Figure S13 in Supporting Information).<sup>22</sup>

#### Solid-State Fluorescence Sensing for Vapor Detection.

The aggregate of **1** was embedded in the PVDF membrane (immersed in an aqueous solution of **1** at  $1.0 \times 10^{-4}$  M for 2 h and then air-dried) to make the vapor detection more practically operational. Prior to sensing studies, it is crucial to first investigate the optical properties of PVDF-embedded **1**. The UV-vis and fluorescence spectra of the PVDF-embedded **1** were recorded, referenced to the spectra in chloroform (Figure 3). The broadened absorption bands and the decreased absorptivities clearly reflect the aggregation state of **1**. Likewise, excited at 490 nm, a new emission band appears at 635 nm, while no monomer emission of **1** (500–600 nm) is observed. The present PVDF-embedded **1** exhibits bathochromic emission in comparison with our previous PBI-bridged bis(permethyl- $\beta$ -CDs) (611 nm),<sup>13a</sup> which is attributed to better exciton coupling due to stronger  $\pi \cdots \pi$  interactions. The average aggregation number of **1** was calculated as 15 in  $1.0 \times 10^{-4}$  M aqueous solution, according to the aggregation constant.<sup>18,23</sup> That is, the averaged 15-stacks of **1** were homogeneously embedded in the PVDF membrane.

The fluorescence of CD-PBI derivatives can be quenched by two factors: one is the photoinduced electron transfer (PET) from analytes to PBI; the other is that encapsulation of analytes disturbs the  $\pi \cdots \pi$  stacking of PBI. The latter is an undesired side effect that can be achieved by common organic reagents. In previous work,<sup>13a,b</sup> the adjacency of CD with PBI by direct junction hindered the  $\pi$ -stacking stability of PBI backbones. The inclusion of analytes into the CD cavity may change the distances between the PBI backbones and thus alter fluorescence, and therefore, a considerable background interference of common organic reagents cannot be neglected during the course of vapor detection. The present CD-PBI conjugate **1** has an elongated junction spacer, which definitely should avoid the background interference. Therefore, several reference reagents were initially tested with the PVDF-embedded **1**, before the detection of the expected amines. As shown in Figure 4, no appreciable fluorescence quenching of PBI was observed when the PVDF-embedded **1** was exposed in the saturated vapors of common organic solvents (methanol, acetonitrile, nitromethane, nitroethane, and toluene), with the exception of chloroform.

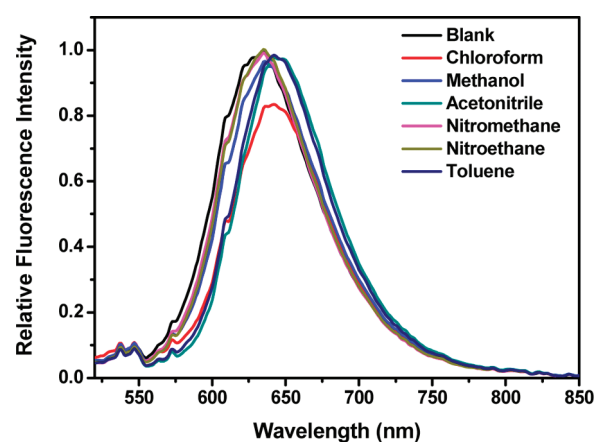


Figure 4. Fluorescence spectra of the PVDF-embedded **1** upon exposure to the saturated vapors of common organic reagents with a response time of 10 s.

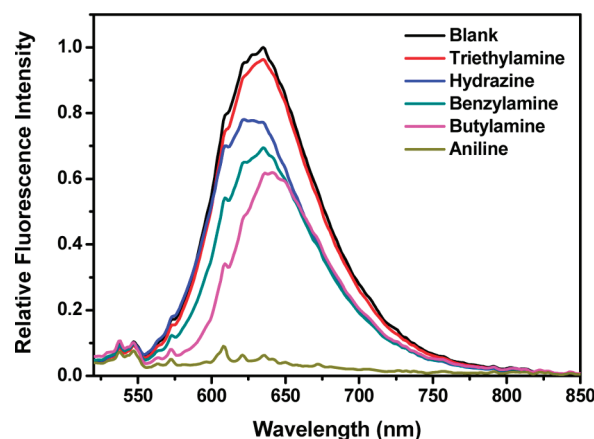


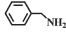
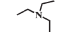
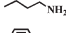
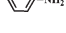
Figure 5. Fluorescence spectra of the PVDF-embedded **1** upon exposure to the saturated vapors of various amines with a response time of 10 s.

Obviously, the anti-interference capability of **1** is dramatically improved in comparison with our previous results.<sup>13a,b</sup> One reasonable explanation is that the compact  $\pi$ -stacking of PBI can hardly be disturbed by the entrapment of common organic reagents. Upon exposure to chloroform, the fluorescence of **1** was quenched to some extent (about 15%). We speculate that such interference is likely due to the good solubility of **1** in chloroform,<sup>24</sup> concurrently considering the high vapor pressure of chloroform (260,000 ppm).

Such negligible background interference is a significant prerequisite for fulfilling highly selective and sensitive vapor detection of amines. On the other hand, the sensing system based on CD-PBI derivatives possesses the advantage of specific binding sites of CD cavities for analytes, which provides a possibility of sensing specialized gaseous molecules utilizing the molecular recognition ability of CDs. The sensing test for the saturated vapors of various amines was performed with a response time of 10 s, including aniline, butylamine, benzylamine, hydrazine, and triethylamine (Figure 5). The corresponding fluorescence quenching efficiencies ( $Q = 1 - I/I_0$ ) were listed in Table 1. Almost no quenching was found upon exposure to triethylamine. Weak to moderate quenching is caused by hydrazine, benzylamine, and butylamine. Most importantly, aniline quenches the



**Table 1.** Fluorescence Response Data of PVDF-Embedded **1** to Saturated Vapors of Various Amines and Corresponding Physical Properties<sup>a–d</sup>

		P (ppm)	E <sub>ox</sub> (V)	Q (%)	R (10 <sup>−5</sup> )	ΔG <sub>PET,M</sub> (eV)	ΔG <sub>PET,A</sub> (eV)
H <sub>2</sub> N–NH <sub>2</sub>	hydrazine	6600 <sup>a</sup>	0.43 <sup>b</sup>	23	3.5	−1.34	−0.97
	benzylamine	950 <sup>a</sup>	1.82 <sup>c</sup>	31	33	0.05	0.42
	triethylamine	76000 <sup>a</sup>	0.99 <sup>b</sup>	4.0	0.053	−0.78	−0.41
	butylamine	120000 <sup>a</sup>	1.52 <sup>c</sup>	39	0.33	−0.25	0.12
	aniline	880 <sup>a</sup>	0.86 <sup>b</sup>	94	110	−0.91	−0.54

<sup>a</sup> Reference 26a. <sup>b</sup> Reference 26b. <sup>c</sup> Reference 26c. <sup>d</sup> P, E<sub>ox</sub>, Q, and R represent the saturated vapor pressure, oxidation potential, quenching efficiency, sensing responsivity, respectively. ΔG<sub>PET,M</sub> and ΔG<sub>PET,A</sub> represent the Gibbs free energy of electron-transfer reaction from the analyte to monomeric and aggregated species of **1**, respectively. It should be noted that because different solvents were employed in electrochemical measurements (methanol for **1** and acetonitrile for amines), there may be errors in the calculation of the Gibbs free-energy changes.

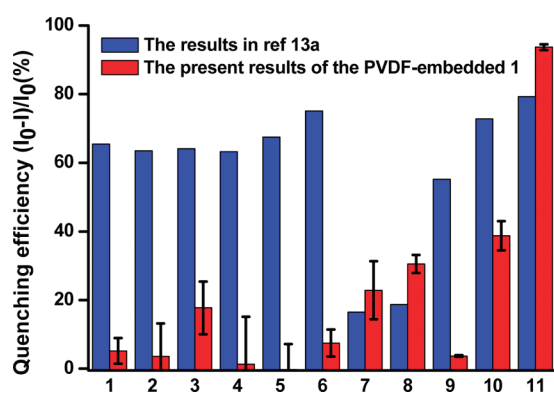


**Figure 6.** Fluorescence response of the PVDF-embedded **1** and PBI-bridged bis(permethyl-β-CDs) **13a** to the saturated vapors of various amines, nitro-based compounds, and general organic solvents with response time of 10 s: 1, toluene; 2, methanol; 3, chloroform; 4, nitromethane; 5, nitroethane; 6, acetonitrile; 7, hydrazine hydrate; 8, benzylamine; 9, triethylamine; 10, butylamine; 11, aniline. Error bar: standard deviation.

fluorescence of **1** nearly in full. The fluorescence quenched by aniline can be attributed to the electron transfer from aniline (electron donor) to the excited **1** (electron acceptor), because the encapsulation of aniline into the cavity of CD decreases distance between PBI fluorophore and aniline, with the result that the electron transfer reaction occurs facily.<sup>2a,3a,6a,13a,13b,25</sup> To the best of our knowledge, it is the first time fluorescence response of solid-state sensory materials has been used to distinguish various amines. In previous works from Zang and our groups,<sup>6a,13a</sup> amine analogues always gave rise to extremely similar responses. A comparison of the sensing results of the PVDF-embedded **1** with those of previous PBI-bridged bis(permethyl-β-CDs) **13a** is shown in Figure 6.

Three factors contribute to the distinguishable fluorescence responses of **1** with different amines: binding affinities, PET efficiencies, and vapor concentrations. Comparing aniline with triethylamine, the sensory selectivity by quenching is 24 times, which is dominantly controlled by the stronger binding affinity of CD for aniline compared with triethylamine, although

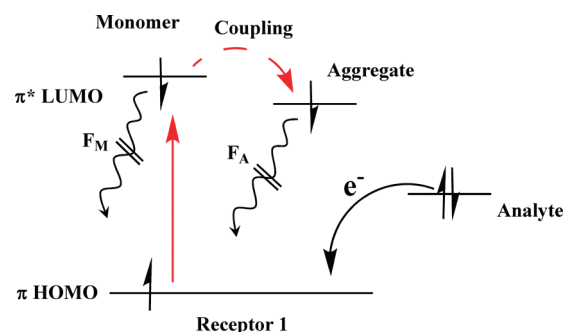


**Figure 7.** Energy level diagram of PET reaction between **1** and analyte.

triethylamine possesses reducing power comparable to that of aniline and vapor concentration over 80 times higher than that of aniline. Aniline and benzylamine are structurally similar, both with an aromatic benzene group; however, the sensory tests show different fluorescence quenching by 3.0 times. Two factors lead to distinct fluorescence quenching upon binding aniline and benzylamine: one is different binding abilities with CD ( $6.7 \times 10^2 \text{ M}^{-1}$  for aniline and  $6.9 \times 10 \text{ M}^{-1}$  for benzylamine),<sup>27</sup> which was further proved by a sensing test of a mixture of aniline and benzylamine (Figure S15 in Supporting Information); the other is that different electron-donor capabilities lead to diverse PET efficiencies. In order to investigate how the electron-donor capability influences the PET efficiency, the Rehm–Weller equation (eq 1) is introduced to estimate the Gibbs free energy (ΔG<sub>PET</sub>) of electron-transfer reaction.

$$\Delta G_{\text{PET}} = e(E_{\text{ox}} - E_{\text{red}}) - E_{00} \quad (1)$$

where  $E_{00}$  is the excited singlet energy of **1**,  $e$  is the electron charge in Coulomb, and  $E_{\text{ox}}$  and  $E_{\text{red}}$  are the oxidation potentials of amines and the first reduction potential of **1**, respectively. We employed the reduction potential of **1** in methanol instead of water (**1** exhibits somewhat weaker  $\pi$ -stacking in methanol than water), obtained as  $E_{\text{red}} = -0.55 \text{ eV}$  (Figure S14 in Supporting Information).<sup>28</sup>  $E_{00}$  can be calculated from the maximum emission wavelength of **1**, 537 nm in monomeric species and 635 nm in aggregated species, respectively. Therefore, with the known parameters  $E_{\text{ox}}$ ,  $E_{\text{red}}$ , and  $E_{00}$ , ΔG<sub>PET</sub> can be calculated according to eq 1; the corresponding data for each electron-transfer system is listed in Table 1. The energy level diagram of PET reaction between **1** and analyte is shown in Figure 7, referencing the previous reports.<sup>6a,29</sup> From the results of ΔG<sub>PET</sub>, aniline is much more likely to quench the fluorescence of **1** than benzylamine. Another emphasis should be on the aniline/butylamine pairs, giving a quenching selectivity of only 2.4. In fact, the real selectivity should be much higher than the observed one when taking the different vapor pressures into account. The vapor pressure is a crucial factor in gas probing, resembling the concentration in solution sensing. Thereby, we defined herein sensing responsivity ( $R$ ) as the quotient of quenching efficiency ( $Q$ ) divided by vapor pressure ( $P$ ), to express the sensing selectivity more definitely (Table 1). With the  $R$  parameter in regard, the sensing capability of **1** for aniline is 2–4 orders of magnitude better than that of other amines (hydrazine, triethylamine, butylamine). It should be noticed that benzylamine affects the specialized probing of aniline to some extent all the time, from the viewpoints of both quenching efficiency and sensing responsivity. As a result, we can determine that the

binding selectivity of CD cavity is the most significant factor influencing the sensing selectivity of **1**.

To examine the detection limit for aniline, the fluorescence quenching efficiency of the PVDF-embedded **1** was carried out at the different vapor pressures of aniline (Figure 8) with a response time of 10 s. The quenching data are well-fitted to the Langmuir equation by hypothesizing that the quenching efficiency is proportional to the surface adsorption (coverage) of aniline. The detection limit of **1** for aniline can be predicted to be as low as 80 ppb from the fitted plot, if the fact that a well-calibrated photodetector can detect intensity change as small as 0.1% or below is considered.<sup>6a,30</sup> The obtained detection limit is satisfactory, benefiting from the amplification effect endowed by the aggregation of **1**. The sensing process is illustrated in Scheme 2. It has been aforementioned that averaged 15-stacks of **1** are

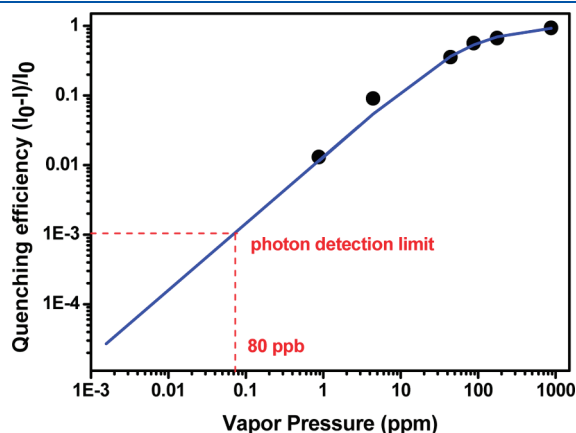


Figure 8. Fluorescence quenching efficiency ( $1 - I/I_0$ ) as a function of the vapor pressure of aniline (data error  $\pm 6\%$ ) fitted with the Langmuir equation.

immersed in PVDF membrane as sensing entities. That is, there are about 30 receptor units (CD cavities) in each sensing entity. The aggregated fluorescence can be substantially quenched when a small portion of receptor sites are filled by the analyte molecules, whereas thorough occupation of all receptor sites is not demanded.

A reversible sensing test of the PVDF-embedded **1** for aniline was performed. The quenched fluorescence can be recovered completely by blowing the membrane with a gas blower for 150 s. The recovered membrane demonstrated the same quenching efficiency when re-exposed to the aniline vapor. Figure 9 shows four continuous cycles of fluorescence quenching–recovery tested with aniline. The PVDF-embedded **1** exhibits excellent

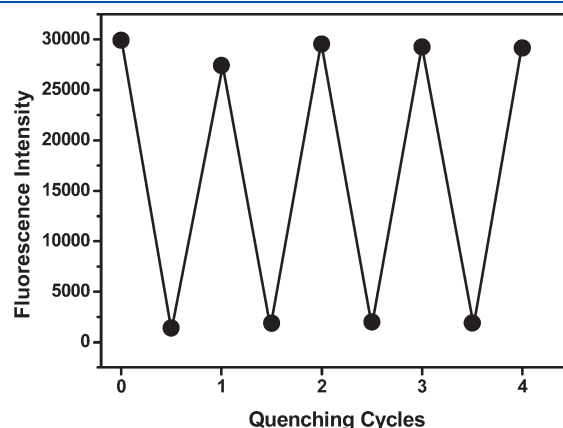
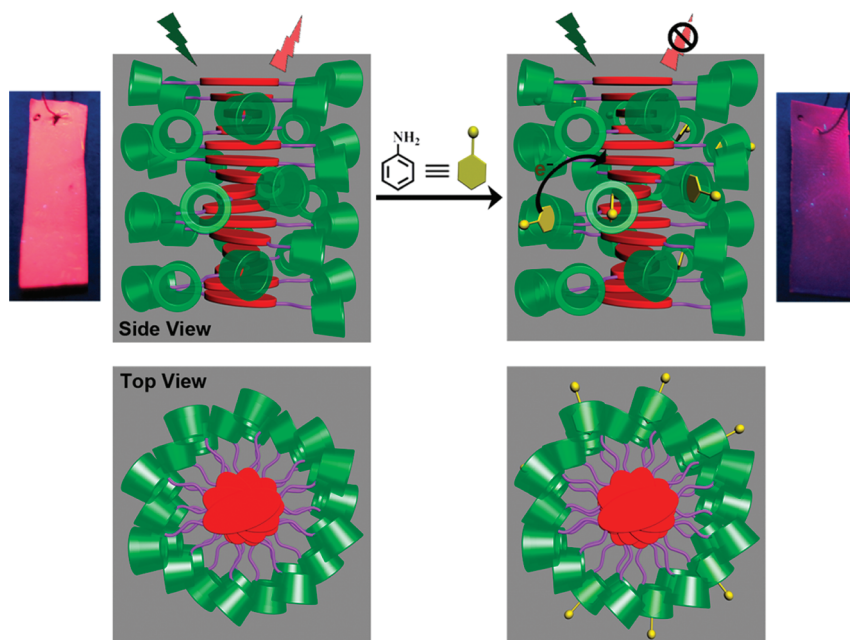


Figure 9. Four continuous cycles of quenching–recovery were tested for the PVDF-embedded **1** upon exposure to the saturated vapor of aniline. The quenching was performed by exposing the membrane to the aniline vapor for 10 s. After each cycle of quenching, the fluorescence of the membrane was recovered by blowing with a gas blower for 150 s.

Scheme 2. Schematic Illustration of the Aggregation Morphology of **1** Embedded in PVDF and Its Sensing Process for Aniline<sup>a</sup>



<sup>a</sup> The left and right photographs represent the fluorescence of the PVDF-embedded **1** before and after exposing to the saturated vapor of aniline with a response time of 10 s (irradiation at 365 nm).

reversibility in the sensing with a quick recovery, which surpasses the previous solid-state fluorescence sensory materials based on PBIs.<sup>6a,13a,13b</sup> Efficient quenching is achieved for the PVDF-embedded **1** over repeated use, implying high stability of  $\pi \cdots \pi$  aggregation of PBIs, where the irreversible fluorescence quenching originated from disturbing the  $\pi$ -stacking of PBI by the entrapment of analytes is avoided. More importantly, the thermodynamically reversible inclusion of CD with analytes contributes dominantly to the sensing reversibility of the PVDF-embedded **1**. The remarkable reversibility means low cost and great convenience, which is a crucial parameter for practical applications of fluorescent sensors and their actual device implementation.

## CONCLUSIONS

In summary, a highly reversible n-type fluorescence sensory supramolecular assembly has been constructed from the CD-PBI conjugate **1**. Comparing with our previous PBI-bridged bis(permethyl- $\beta$ -CDs), **1** with an elongated junction spacer between CD and PBI exhibits much stronger aggregation capability because the longer spacer can avoid the steric hindrance of CD to the PBI  $\pi$ -stacking. The membrane-embedded **1** in PVDF has demonstrated compelling selectivity and sensitivity in detection of amine vapors because it gathers together the following features: (i) its strong  $\pi$ -stacking overcomes the background interference; (ii) it exhibits high selectivity to aniline, benefiting from the diverse binding ability of CD; (iii) the PVDF-embedded **1** is conveniently prepared and practically operational; (iv) it exhibits excellent reversibility in the sensing with a quick recovery. A combination of these four characteristics promises the design and construction of smart supramolecular materials, feasibly applied to probing aniline instantly.

## EXPERIMENTAL SECTION

**Materials.** All chemicals used were reagent grade unless noted otherwise. Glycine, trifluoroacetic acid, and perylene-3,4,9,10-tetracarboxylic acid dianhydride were purchased from commercial resources and used without further purification. 6-Deoxy-6-amino-permethyl- $\beta$ -cyclodextrin was synthesized according to the procedure in the literature from natural  $\beta$ -cyclodextrin.<sup>14</sup> *N*-(*tert*-butoxycarbonyl)-glycine was synthesized and purified according to the reported procedures.<sup>15</sup> The poly(vinylidene fluoride) (PVDF) membrane (Immobilon-P, IPVH00010, and 0.45  $\mu$ m) was purchased from a commercial resource.

**Synthesis of 6-Deoxy-6-(*N*-(*tert*-butoxycarbonyl))-glycinamide-permethyl- $\beta$ -cyclodextrin (P1).** 6-Deoxy-6-amino-permethyl- $\beta$ -cyclodextrin (2.1 g, 1.48 mmol) and triethylamine (450 mg, 4.45 mmol) were dissolved in dry THF (60 mL). After the mixture was placed in an ice bath, *N*-(*tert*-butoxycarbonyl)-glycine (259 mg, 1.48 mmol), DCC (304 mg, 1.48 mmol), and HOBT (241 mg, 1.48 mmol) were added. The resultant mixture was allowed to warm to room temperature and stirred under N<sub>2</sub> overnight. The solvent was removed at reduced pressure, and the residue was dissolved in dichloromethane (DCM), washed with water, dried over Na<sub>2</sub>SO<sub>4</sub>, and evaporated to dryness under vacuum. The residue was purified by silica gel column chromatography using chloroform/methanol (35:1 v/v) as the eluent to give the product as a white powder (1543 mg) in a yield of 65%. <sup>1</sup>H NMR (CDCl<sub>3</sub>, 400 MHz, ppm):  $\delta$  6.51 (s, 1 H), 5.34 (s, 1 H), 5.17–5.10 (m, 7 H), 3.85–3.39 (m, 104 H), 1.45 (s, 9 H). <sup>13</sup>C NMR (75 MHz, CDCl<sub>3</sub>, ppm):  $\delta$  169.2, 155.8, 98.8, 98.6, 98.3, 81.9, 81.7, 81.5, 81.4, 81.2, 80.3, 80.1, 80.0, 79.8, 79.7, 77.7, 77.3, 76.8, 71.3, 71.2, 70.9, 70.8, 70.2, 61.2, 59.2, 58.8, 58.3, 58.2, 44.2, 40.2, 28.2. MS: [M + Na<sup>+</sup>] for 1593.8. Anal.

Calcd for C<sub>69</sub>H<sub>122</sub>N<sub>2</sub>O<sub>37</sub>: C 52.73, H 7.82, N 1.78. Found: C 52.70, H 7.87, N 1.70.

**Synthesis of 6-Deoxy-6-glycinamide-permethyl- $\beta$ -cyclodextrin (P2).** 6-Deoxy-6-(*N*-(*tert*-butoxycarbonyl))-glycinamide-permethyl- $\beta$ -cyclodextrin (1250 mg, 0.80 mmol) was dissolved in DCM (8 mL), and then trifluoroacetic acid (2 mL) was added. The mixture was stirred at room temperature overnight. The solvent was removed at reduced pressure and afforded a primrose yellow solid (1160 mg) in 91% yield. <sup>1</sup>H NMR (CDCl<sub>3</sub>, 400 MHz, ppm):  $\delta$  5.11–5.04 (m, 7 H), 3.80–3.19 (m, 104 H). <sup>13</sup>C NMR (75 MHz, CDCl<sub>3</sub>, ppm):  $\delta$  99.5, 99.4, 99.0, 81.9, 82.1, 81.8, 81.6, 81.3, 81.1, 80.5, 79.7, 77.5, 77.3, 77.1, 76.6, 71.6, 71.5, 71.4, 71.0, 70.5, 69.8, 61.4, 61.2, 59.5, 59.0, 58.9, 58.7, 58.6, 58.5, 58.4, 41.1, 40.4. MS: [M + H<sup>+</sup>] for 1471.4. Anal. Calcd for C<sub>64</sub>H<sub>114</sub>N<sub>2</sub>O<sub>35</sub>·CF<sub>3</sub>COOH: C 49.99, H 7.31, N 1.77. Found: C 49.82, H 7.49, N 1.60.

**Synthesis of Perylene Bisimide-Bridged Bis(permethyl- $\beta$ -cyclodextrins) (1).** 6-Deoxy-6-glycinamide-permethyl- $\beta$ -cyclodextrin (900 mg, 0.56 mmol), perylene-3,4,9,10-tetracarboxylic acid bisanhydride (110 mg, 0.28 mmol), zinc acetate (50 mg, 0.28 mmol), and imidazole (8.0 g) were mixed. The reaction mixture was heated at 140 °C under N<sub>2</sub> for 6 h. After cooling to room temperature, the mixture was dissolved in DCM, washed with a solution of HCl (1 mol/L), dried over Na<sub>2</sub>SO<sub>4</sub>, and evaporated to dryness under vacuum. The residue was purified by silica gel column chromatography using chloroform/methanol (30:1 v/v) as the eluent to give the product as a red powder (320 mg) at yield of 34%. <sup>1</sup>H NMR (CDCl<sub>3</sub>, 400 MHz, ppm):  $\delta$  8.67 (q, 8 H), 5.19–4.98 (m, 18 H), 3.68–3.38 (m, 204 H). <sup>13</sup>C NMR (100 MHz, CDCl<sub>3</sub>, ppm):  $\delta$  167.5, 163.8, 135.5, 132.3, 130.3, 127.2, 123.9, 123.8, 99.7, 99.6, 99.4, 82.8, 82.7, 82.5, 82.2, 81.3, 81.0, 80.9, 80.8, 78.0, 77.9, 77.7, 77.4, 72.2, 71.9, 71.8, 71.7, 71.6, 70.8, 62.3, 62.2, 62.1, 62.0, 61.9, 60.1, 59.8, 59.7, 59.6, 59.5, 59.3, 59.1, 43.8, 40.9. MALDI-MS: [M + Na<sup>+</sup>] for 3321.438. Anal. Calcd for C<sub>152</sub>H<sub>232</sub>N<sub>4</sub>O<sub>74</sub>: C 55.33, H 7.09, N 1.70. Found: C 55.03, H 7.41, N 1.65.

**PVDF-Embedded 1 and Solid-State Fluorescence Sensing Experiments.** The solid-state fluorescence sensing experiments were performed as follows: (i) The PVDF membrane was immersed in 1.0  $\times$  10<sup>−4</sup> M **1** in aqueous solution for 2 h, and then the PVDF membrane was air-dried and tailored to the proper size based on the front surface accessory on a fluorescence spectrometer. (ii) The solid-state fluorescence spectra were measured immediately after immersion inside a sealed jar (100 mL) containing small amount of amines or common organic solvents. Before using, the jar was sealed overnight to achieve saturated vapor inside. The exposure time was determined by stopwatch. The detection limit experiment was performed as follows: Injection of 0.05 mL of the saturated aniline vapor (880 ppm) into a 10 mL sealed jar produced a vapor pressure of 4.4 ppm. A vapor pressure of 0.88 ppm was obtained according to the following steps: (i) Injection of 1.00 mL of the saturated aniline vapor (880 ppm) into a 10 mL sealed jar produced a vapor pressure of 88 ppm. (ii) A 0.10 mL portion of aniline vapor (88 ppm) was injected into a 10 mL sealed jar, producing a vapor pressure of 0.88 ppm. All solid-state fluorescence sensing experiments were performed for three times, and the data used in the paper are a average of experiment data.

**Cyclic Voltammetric (CV) Measurement.** The methanol solution of **1** was prepared in dry methanol containing 0.1 M Bu<sub>4</sub>NClO<sub>4</sub> as a supporting electrolyte. The solution was purged for at least 10 min with solvent-saturated nitrogen. The electrochemical measurement was performed at a Pt working electrode with a Pt wire counter electrode, and Ag/AgCl was added to the solution as a reference electrode. The oxidation potential for Ag/AgCl was taken as −0.02 V vs SCE.

## ASSOCIATED CONTENT

**S Supporting Information.** NMR and MALDI-MS spectra of **1** and other data as described in the text. This material is available free of charge via the Internet at <http://pubs.acs.org>.



## AUTHOR INFORMATION

## Corresponding Author

\*E-mail: yuliu@nankai.edu.cn.

## ACKNOWLEDGMENT

This work was supported by 973 Program (2011CB932502), NNSFC (No. 20932004), which are gratefully acknowledged.

## REFERENCES

- (1) Zhou, Q.; Swager, T. M. *J. Am. Chem. Soc.* **1995**, *117*, 7017–7018.
- (2) (a) Thomas, S. W., III; Joly, G. D.; Swager, T. M. *Chem. Rev.* **2007**, *107*, 1339–1386. (b) Kim, H. N.; Guo, Z.; Zhu, W.; Yoon, J.; Tian, H. *Chem. Soc. Rev.* **2011**, *40*, 79–93. (c) Zang, L.; Che, Y.; Moore, J. S. *Acc. Chem. Res.* **2008**, *41*, 1596–1608.
- (3) (a) Swager, T. M. *Acc. Chem. Res.* **2008**, *41*, 1181–1189. (b) Toal, S. J.; Trogler, W. C. *J. Mater. Chem.* **2006**, *16*, 2871–2883. (c) McQuade, D. T.; Pullen, A. E.; Swager, T. M. *Chem. Rev.* **2000**, *100*, 2537–2574.
- (4) (a) Naddo, T.; Che, Y.; Zhang, W.; Balakrishnan, K.; Yang, X.; Yen, M.; Zhao, J.; Moore, J. S.; Zang, L. *J. Am. Chem. Soc.* **2007**, *129*, 6978–6979. (b) Ding, L.; Fang, Y. *Chem. Soc. Rev.* **2010**, *39*, 4258–4273.
- (5) Newman, C. R.; Frisbie, C. D.; da Silva Filho, D. A.; Bredas, J.-L.; Ewbank, P. C.; Mann, K. R. *Chem. Mater.* **2004**, *16*, 4436–4451.
- (6) (a) Che, Y.; Yang, X.; Loser, S.; Zang, L. *Nano Lett.* **2008**, *8*, 2219–2223. (b) Che, Y.; Zang, L. *Chem. Commun.* **2009**, 5106–5108.
- (7) Tang, Z.; Yang, J.; Yu, J.; Cui, B. *Sensors* **2010**, *10*, 6463–6476.
- (8) (a) Hernández-Jover, T.; Izquierdo-Pulido, M.; Veciana-Nogués, M. T.; Vidal-Carou, M. C. *J. Agric. Food Chem.* **1996**, *44*, 2710–2715. (b) Hernández-Jover, T.; Izquierdo-Pulido, M.; Veciana-Nogués, M. T.; Vidal-Carou, M. C. *J. Agric. Food Chem.* **1996**, *44*, 3097–3101. (c) Hernández-Jover, T.; Izquierdo-Pulido, M.; Veciana-Nogués, M. T.; Mariné-Font, A.; Vidal-Carou, M. C. *J. Agric. Food Chem.* **1997**, *45*, 2098–2102. (d) Veciana-Nogués, M. T.; Mariné-Font, A.; Vidal-Carou, M. C. *J. Agric. Food Chem.* **1997**, *45*, 4324–4328.
- (9) Muir, D. D.; Hunter, E. A.; Banks, J. M. *Milchwissenschaft* **1997**, *52*, 85–88.
- (10) Preti, G.; Labows, J. N.; Kostelc, J. G.; Aldinger, S.; Daniele, R. *J. Chromatogr. Biomed. Appl.* **1988**, *432*, 1–11.
- (11) (a) Sotzing, G. A.; Phend, J. N.; Grubbs, R. H.; Lewis, N. S. *Chem. Mater.* **2000**, *12*, 593–595. (b) Simenhoff, M. L.; Burke, J. F.; Saukkonen, J. J.; Ordinario, A. T.; Doty, R. N. *Engl. J. Med.* **1977**, *297*, 132–135.
- (12) Chow, C.-F.; Kong, H.-K.; Leung, S.-W.; Chiu, B. K. W.; Koo, C.-K.; Lei, E. N. Y.; Lam, M. H. W.; Wong, W.-T.; Won, W.-Y. *Anal. Chem.* **2011**, *83*, 289–296.
- (13) (a) Liu, Y.; Wang, K.-R.; Guo, D.-S.; Jiang, B.-P. *Adv. Funct. Mater.* **2009**, *19*, 2230–2235. (b) Jiang, B.-P.; Guo, D.-S.; Liu, Y. *J. Org. Chem.* **2010**, *75*, 7258–7264. (c) Wang, F.; Yang, Y.; Swager, T. M. *Angew. Chem., Int. Ed.* **2008**, *47*, 8394–8396.
- (14) Reetz, M. T.; Waldvogel, S. R. *Angew. Chem., Int. Ed.* **1997**, *36*, 865–867.
- (15) Kommidi, H.; Balasubramaniam, S.; Aidhen, I. S. *Tetrahedron* **2010**, *66*, 3723–3729.
- (16) (a) Würthner, F. *Chem. Commun.* **2004**, 1564–1579. (b) Chen, Z.; Lohr, A.; Saha-Möller, C. R.; Würthner, F. *Chem. Soc. Rev.* **2009**, *38*, 564–584.
- (17) (a) Szejtli, J. *Chem. Rev.* **1998**, *98*, 1743–1753. (b) Rekharsky, M. V.; Inoue, Y. *Chem. Rev.* **1998**, *98*, 1875–1918. (c) Liu, Y.; Chen, Y. *Acc. Chem. Res.* **2006**, *39*, 681–691. (d) Connors, K. A. *Chem. Rev.* **1997**, *97*, 1325–1357.
- (18) Würthner, F.; Thalacker, C.; Diele, S.; Tschierske, C. *Chem.—Eur. J.* **2001**, *7*, 2245–2253.
- (19) Wang, K.-R.; Guo, D.-S.; Jiang, B.-P.; Sun, Z.-H.; Liu, Y. *J. Phys. Chem. B* **2010**, *114*, 101–106.
- (20) (a) Wang, W.; Li, L.-S.; Helms, G.; Zhou, H.-H.; Li, A. D. Q. *J. Am. Chem. Soc.* **2003**, *125*, 1120–1121. (b) Li, A. D. Q.; Wang, W.; Wang, L.-Q. *Chem.—Eur. J.* **2003**, *9*, 4594–4601. (c) Shaller, A. D.; Wang, W.; Gan, H.; Li, A. D. Q. *Angew. Chem., Int. Ed.* **2008**, *47*, 7705–7709.
- (21) (a) Graser, F.; Hädicke, E. *Liebigs Ann. Chem.* **1980**, 1994–2011. (b) Klebe, G.; Graser, F.; Hädicke, E.; Berndt, J. *Acta Crystallogr., Sect. B: Struct. Sci.* **1989**, *45*, 69–77.
- (22) Li, X.-Q.; Zhang, X.; Ghosh, S.; Würthner, F. *Chem.—Eur. J.* **2008**, *14*, 8074–8078.
- (23) Chen, Z.; Stepanenko, V.; Dehm, V.; Prins, P.; Siebbeles, L. D. A.; Seibt, J.; Marquetand, P.; Engel, V.; Würthner, F. *Chem.—Eur. J.* **2007**, *13*, 436–449.
- (24) Che, Y.; Yang, X.; Liu, G.; Yu, C.; Ji, H.; Zuo, J.; Zhao, J.; Zang, L. *J. Am. Chem. Soc.* **2010**, *132*, 5743–5750.
- (25) Yang, J.-S.; Swager, T. M. *J. Am. Chem. Soc.* **1998**, *120*, 5321–5322.
- (26) (a) The vapor pressure data are cited from *CRC Handbook of Chemistry and Physics*, 85th ed.; CRC Press: Boca Raton, 2004. (b) Weinberg, N. L.; Weinberg, H. R. *Chem. Rev.* **1968**, *68*, 449–523. (c) Barnes, K. K.; Mann, C. K. *J. Org. Chem.* **1967**, *32*, 1474–1479.
- (27) (a) Velusamy, P.; Pitchumani, K.; Srinivasan, C. *Tetrahedron* **1996**, *52*, 3487–3496. (b) Gadosy, T. A.; Boyd, M. J.; Tee, O. S. *J. Org. Chem.* **2000**, *65*, 6879–6889.
- (28) We have tried several times to obtain the reduction potential of **1** in water, but all failed, where no peak was observed, probably because **1** forms a bulky aggregate, inhibiting the electrochemical diffusion and signal formation.
- (29) Clark, A. E.; Qin, C.; Li, A. D. Q. *J. Am. Chem. Soc.* **2007**, *129*, 7586–7595.
- (30) Cumming, C. J.; Aker, C.; Fisher, M.; Fox, M.; Grone, M. J. I.; Reust, D.; Rockley, G.; Swager, T. M.; Towers, E.; Williams, V. *IEEE Trans. Geosci. Remote Sensing* **2001**, *39*, 1119–1128.